Dot1L interacts with Zc3h10 to activate UCP1 transcription and promote thermogenesis

Danielle Yi[1,2], Hai P. Nguyen[1,2], Jennie Dinh[1], Jose A. Viscarra[1], Ying Xie[1], Jon M. Dempersmier[1], Yuhui Wang[1], and Hei Sook Sul[1,2,3]

Department of Nutritional Sciences & Toxicology[1], Endocrinology Program[2], University of California, Berkeley, CA 94720

[3]Corresponding author: hsul@berkeley.edu

ABSTRACT

Brown adipose tissue is a metabolically beneficial organ capable of dissipating chemical energy into heat, thereby increasing energy expenditure. Here, we identify Dot1L, the only known H3K79 methyltransferase, as an interacting partner of Zc3h10 that transcriptionally activates the UCP1 promoter and other BAT genes. Through a direct interaction, Dot1L is recruited by Zc3h10 to the promoter regions of thermogenic genes to function as a coactivator by methylating H3K79. We also show that Dot1L is induced during brown fat cell differentiation and by cold exposure and that Dot1L and its H3K79 methyltransferase activity is required for thermogenic gene program. Furthermore, we demonstrate that Dot1L ablation in mice using UCP1-Cre prevents activation of UCP1 and other target genes to reduce thermogenic capacity and energy expenditure, promoting adiposity. Hence, Dot1L plays a critical role in the thermogenic program and may present as a future target for obesity therapeutics.

INTRODUCTION

Adipose tissue has a central role in controlling mammalian energy metabolism in that, while white adipose tissue (WAT) is to store excess calories, brown adipose tissue (BAT) is to dissipate energy via non-shivering thermogenesis (Cannon and Nedergaard, 2004). Classic brown adipocytes contain a high density of mitochondria that contain Uncoupling protein 1 (UCP1), which uncouples respiration from ATP synthesis and generates heat instead (Farmer, 2008, Cannon and Nedergaard, 2004). In addition, beige/brite adipocytes in WAT depot are recruited upon cold exposure or β_3-adrenergic stimulation (Seale et al., 2008, Wang and Seale, 2016, Sanchez-Gurmaches et al., 2016, Cypess et al., 2009, Lichtenbelt et al., 2009, Virtanen et al., 2009, Chondronikola et al., 2014). Based on several cross-sectional studies, adult human brown fat or brown fat-like tissue is inversely correlated with body mass index and visceral fat (Lichtenbelt et al., 2009, Hibi et al., 2016, Jimenez et al., 2007). Therefore, unraveling the mechanisms underlying the thermogenic gene program has drawn growing attention in obesity research as a promising avenue to combat obesity and associated metabolic diseases.

One of the major advances in BAT biology has been understanding the transcription network that governs the thermogenic gene program and finding critical factors that activate the UCP1 gene. A multitude of transcriptional regulators have been implicated in the transcription of UCP1, including transcription factors, Zfp516, IRF4 and EBF2, and transcriptional coregulators, PRDM16, PGC1α and LSD1 (Seale et al., 2008, Rajakumari et al., 2013, Dempersmier et al., 2015, Puigserver et al., 1998, Sambeat et al., 2016, Kong et al., 2014). Recently, we identified a BAT-enriched and cold-induced transcription factor, Zc3h10 that activates the UCP1 and other target genes, such as Tfam and Nrf1 for mitochondrial biogenesis (Yi et al., 2019). Zc3h10 activates the UCP1 promoter by directly binding to the -4.6 kb region. Upon sympathetic stimulation, Zc3h10 is phosphorylated at S126 by p38 mitogen-activated protein kinase (MAPK) to increase binding to this distal region of the UCP1 promoter. Consequently, Zc3h10 ablation in

mice impairs the thermogenic gene program, while Zc3h10 overexpression in adipose tissue enhances the thermogenic capacity and energy expenditure, protecting mice from diet-induced obesity (Yi et al., 2019).

As in most biological processes, BAT as well as beige fat, rely heavily on environmental cues for its full activation of the thermogenic gene program. Integrating epigenetic effectors into the thermogenic network may provide a comprehensive understanding in the regulation of thermogenic gene program (Yi et al., 2020). Here, we identify Dot1L (disruptor of telemetric silencing 1-like) as an interacting partner of Zc3h10 and a critical coactivator of thermogenic genes. Dot1L is the only known methyltransferase that catalyzes the sequential mono-, di- and tri-methylation of H3K79, which, unlike major epigenetic sites, is located at the globular domain of nucleosome (Min et al., 2003, van Leeuwen et al., 2002, Frederiks et al., 2008). Differing from other histone methyltransferases, Dot1L does not contain a SET domain but uniquely has an AdoMET motif (Feng et al., 2002, van Leeuwen et al., 2002). Dot1L is broadly known to play roles in telomere silencing, cell cycle regulations and is particularly well studied in mixed lineage leukemia (MLL)-related leukemogenesis (Schulze et al., 2009, Okada et al., 2005, Nguyen and Zhang, 2011, Ng et al., 2002). However, not much is known about Dot1L recruitment to specific sites by specific transcription factors. Nor the role of Dot1L is thermogenic gene program is known.

We show here that Dot1L is recruited to the UCP1 promoter region via its direct interaction to Zc3h10 for Zc3h10-mediated transcriptional activation at the UCP1 and other target genes. By using the specific and potent chemical inhibitor of Dot1L-H3K79 methyltransferase activity, pinometostat (EPZ-5676), we demonstrate that Dot1L methyltransferase activity is required for thermogenic gene expression in vitro and in vivo. Moreover, Dot1L ablation in brown adipocytes impairs the thermogenic program, whereas ectopic Dot1L expression enhances and thermogenic gene program. Dot1L ablation in UCP1^{+} cells in mice impairs the thermogenic capacity and lowers oxygen consumption, leading to weight gain. In this regard, the GWAS database reveals multiple SNPs of Dot1L associated with a waist-hip ratio and body mass index, further supporting a potential role of Dot1L in human obesity (GWAS Central identifier: HGVPM1111, HGVPM1114).

RESULTS

Dot1L is recruited by Zc3h10 for activation of BAT gene program

We previously reported Zc3h10 as a BAT-enriched transcription factor that promotes the BAT gene program (Yi et al., 2019). Most transcription factors do not work alone but rather form a complex to recruit other cofactors for transcription. Thus, as a DNA-binding protein, Zc3h10 may interact with coregulators to activate BAT gene transcription. Therefore, we searched for potential interacting partners of Zc3h10. The Zc3h10 with the streptavidin- and calmodulin-binding epitope-tag were incubated with nuclear extracts from BAT and the Zc3h10 complex after sequential purification were subjected to mass spectrometry. We identified multiple potential Zc3h10 interacting proteins, among which were methyltransferases and chromatin remodelers (Supplementary Figure 1A). For further studying as a Zc3h10 interacting protein, we selected Dot1L (disruptor of telemetric silencing 1-like), the H3K79 methyltransferase, as it directly interacted with Zc3h10 and was the only BAT enriched gene out of the candidates tested.

First, for validation of interaction between Dot1L and Zc3h10, we performed Co-IP experiments with lysates of HEK293FT cells transfected with HA-Dot1L and Flag-Zc3h10 by using FLAG and HA antibodies. Indeed, we detected FLAG-Zc3h10 upon immunoprecipitation with HA antibodies. Conversely, HA-Dot1L was detected upon immunoprecipitation with FLAG antibodies (Figure 1A, left). We then tested an interaction of the two endogenous proteins using BAT from mice. Again, we detected the presence of endogenous Zc3h10 when nuclear extracts

103 of BAT from mice were immunoprecipitated with Dot1L antibody. By reverse Co-IP, we
104 confirmed the interaction between endogenous Dot1L and Zc3h10 (Figure 1A, right). We next
105 asked whether Dot1L can directly bind Zc3h10, by using glutathione S-transferase (GST) fused
106 to Dot1L expressed and purified from *E. Coli* (Supplementary Figure 1B). Incubation of GST-
107 Dot1L fusion protein immobilized on glutathione beads with *in vitro* transcribed and translated
108 [^{35}S]-Zc3h10, but not control GST-alone, detected the presence of Zc3h10 (Figure 1B). Overall,
109 these results demonstrate that Dot1L directly interacts with Zc3h10. We next examined domains
110 of Dot1L for its interaction with Zc3h10. We generated three Dot1L truncated constructs; N-
111 terminal Dot1L (1-500aa) containing the catalytic domain, the middle fragment (501-1000aa)
112 containing the coiled-coil domain, and the C-terminal domain (1001-1540aa); All constructs
113 were N-terminally tagged with HA. We then cotransfected these constructs with full-length Flag-
114 tagged Zc3h10. By Co-IP, we detected the middle fragment (501 -1000) of Dot1L, that contains
115 coiled coil motifs, interacting with Zc3h10, but not the other two regions of Dot1L (Figure 1C).
116 We conclude that the middle fragments of Dot1L contains the Zc3h10 interacting domain.
117 Since Zc3h10 activates UCP1 and other target genes for BAT gene program and Dot1L
118 interacts with Zc3h10, Dot1L expression pattern could be similar to Zc3h10 and thus BAT-
119 enriched. Indeed, tissue expression profiling by RT-qPCR and immunoblotting showed that
120 Dot1L was enriched in mouse BAT compared to other tissues tested, such as WAT, liver and
121 stomach (Figure 1D). We next compared Dot1L mRNA levels between the stromal vascular
122 fraction (SVF) that contains preadipocytes with adipocyte fraction of BAT from 10-wk-old wild-
123 type (WT) mice. As expected, UCP1 was enriched in the adipocyte fraction, whereas PDGFRα
124 expression was higher in the SVF fraction. We found Dot1L to be enriched in the brown
125 adipocyte fraction by over 2-fold compared to the SVF (Figure 1E, left). Moreover, similar to
126 Zc3h10, expression of Dot1L in BAT was induced upon cold exposure (Figure 1E, right). We
127 next examined Dot1L expression during BAT cell differentiation in vitro. During the course of
128 brown adipocyte differentiation, as expected, UCP1 expression was induced, whereas
129 expression of preadipocyte gene, Pref-1, was suppressed. More importantly, similar to Zc3h10,
130 Dot1L mRNA level was increased during BAT cell differentiation (Figure 1F). Overall, we
131 conclude that Dot1L expression pattern is similar to Zc3h10 in terms of enrichment in mature
132 brown adipocytes and induction by cold exposure, which may allow potential a cooperative
133 function of Dot1L and Zc3h10 for the BAT gene program.
134 Next, to examine the functional significance of Dot1L and Zc3h10 interaction in the
135 activation of UCP1 promoter, we performed the luciferase (Luc) reporter assay using the -5.5 kb
136 UCP1-Luc promoter. Along with the UCP1 promoter-Luc construct, Zc3h10 and Dot1L were
137 cotransfected into HEK293 cells. As expected, compared to empty vector control, Zc3h10 alone
138 activated the UCP1 promoter over 3-fold. Dot1L alone could not activate the UCP1 promoter.
139 When co-transfected with Zc3h10, Dot1L was able to synergistically activate the UCP1
140 promoter, resulting in a robust 11-fold increase in the UCP1 promoter activity (Figure 1G, left).
141 These results demonstrate the cooperative function of Dot1L and Zc3h10 in UCP1 promoter
142 activation. Next, because Dot1L interacts with Zc3h10 to enhance the UCP1 promoter activity,
143 we predicted that Dot1L should occupy the same UCP1 promoter region where Zc3h10 binds.
144 We performed chromatin immunoprecipitation (ChIP) using BAT cells transduced with
145 adenovirus containing Flag- tagged Zc3h10 and HA-tagged Dot1L. By using Flag (for Zc3h10)
146 and HA (for Dot1L) antibodies, we detected strong enrichment of both Zc3h10 and Dot1L at the
147 - 4.6 kb region of the UCP1 promoter, a region corresponding to the Zc3h10 binding site (Yi et
148 al., 2019) (Figure 1G, right). This illustrates co-occupancy of Dot1L and Zc3h10 at the same
149 region of the UCP1 promoter. Collectively, we demonstrate that Dot1L, as an interacting partner
150 of Zc3h10, is a critical coactivator of the UCP1 promoter.
151

Figure 1. Dot1L directly interacts with Zc3h10 for UCP1 promoter activation

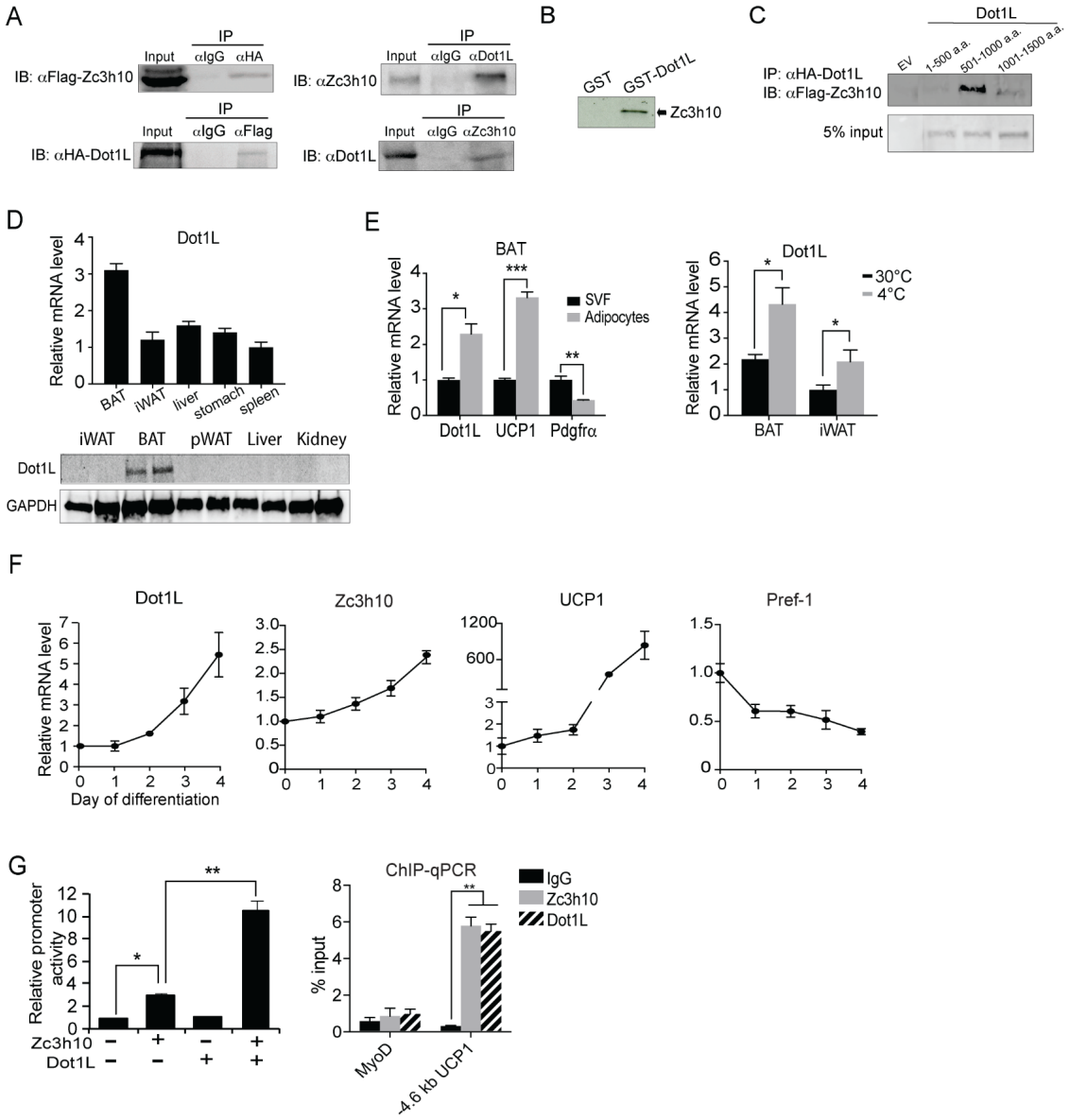

Figure 1. Dot1L directly interacts with Zc3h10 for UCP1 promoter activation

(A) (Left) CoIP using αFlag for Zc3h10 or αHA for Dot1L after IP with either αHA- or αFlag, respectively, using lysates from HEK293FT cells transfected with Flag-Zc3h10 and HA-Dot1L. (Right) CoIP of endogenous Zc3h10 and Dot1L using BAT tissue of C57BL/6 using αZc3h10 and αDot1L.

(B) Autoradiograph of GST pull-down using GST-Dot1L and ^{35}S-labeled in vitro transcribed/ translated Zc3h10.

(C) CoIP using αFlag for Zc3h10 after IP with αHA for Dot1L using lysates from HEK293FT cells transfected with Flag-Zc3h10 and various HA-Dot1L constructs.

(D) RT-qPCR and immunoblotting of Dot1L in various tissues from 10-wk-old C57BL/6 mice.

(E) (Left) RT-qPCR for indicated genes in the adipocyte fraction and SVF from BAT. (Right) RT-qPCR for Dot1L mRNA of BAT and iWAT from mice housed at either 30°C or 4°C (n=4).

(F) RT-qPCR for indicated genes during BAT cell differentiation.

(G) (Left) HEK293FT cells were cotransfected with the -5.5 kb UCP1-Luc promoter with Zc3h10 or Dot1L alone or together. (Right) ChIP-qPCR for Zc3h10 and Dot1L enrichment at the -4.6 kb region of UCP1 promoter using Flag or HA antibodies. Differentiated BAT cells transduced with either Flag-Zc3h10 or HA-Dot1L were used.

Dot1L promotes the thermogenic gene program in vitro

We next tested whether Dot1L is required for BAT gene program in cultured BAT cells. BAT cells at Day 2 of differentiation were transduced with adenovirus expressing short hairpin RNAs targeting Dot1L for knockdown (Dot1L KD). Transduction of shDot1L adenovirus in BAT cells caused a decrease in Dot1L mRNA levels by approximately 60% (Figure 2A, left). While there were no apparent changes in expression of transcription factors critical for brown adipocyte differentiation, such as PPARγ, there was a 50% reduction of UCP1 expression at mRNA and protein levels (Figure 2A). Expression of other Zc3h10 target genes, including Tfam, Nrf1 and Elovl3, was also decreased significantly (Figure 2A, middle). Moreover, Dot1L KD BAT cells had decreased oxygen consumption rate (OCR) in oligomycin-, FCCP-, and rotenone/antimycin A-treated conditions (Figure 2B, left). Notably, the uncoupled respiration of Dot1L KD cells was significantly lower than the control BAT cells in both basal and in forskolin-treated stimulated conditions (Figure 2B, right). These results suggest that Dot1L is critical for full activation of the BAT gene program and mitochondriogenesis, and thus thermogenic function in BAT cells.

Next, in order to further establish the role for Dot1L in BAT gene program, we treated BAT cells with a specific inhibitor of Dot1L H3K79 methyltransferase, EPZ5676. We predicted that if Dot1L is required for the transcriptional activation of UCP1 and other BAT genes, inhibition of Dot1L activity should prevent BAT gene expression. Dot1L inhibition resulted in a significant reduction in mRNA and protein levels for UCP1 by 90% (Figure 2C). Expression of other BAT-enriched Zc3h10 target genes, such as Tfam, Nrf1, Cox7a and Cox8b, was decreased by 40-80%, whereas PPARγ expression was not affected (Figure 2C). These results show that Dot1L methyltransferase activity is required for thermogenic gene expression and other Zc3h10 target genes for the BAT gene program.

We then tested the ability of Dot1L to induce UCP1 and other thermogenic genes by gain of function experiment. We overexpressed Dot1L or Zc3h10 alone or together via adenoviral transduction in 3T3-L1 cells and the cells were induced to browning by forskolin treatment. We first verified Zc3h10 and Dot1L overexpression by RT-qPCR and immunoblotting (Figure 2D, top). Interestingly, Dot1L overexpression alone increased UCP1 mRNA levels over 2-fold, probably due to the presence of endogenous Dot1L in 3T3-L1 cells. Co-overexpression of both Dot1L and Zc3h10 resulted in a further increase in UCP1 mRNA levels by 3-fold. (Figure 2D, bottom). Furthermore, overexpression of Dot1L and Zc3h10 together in differentiated 3T3- L1 cells further increased mRNA levels for Tfam and Nrf1 in comparison to Dot1L or Zc3h10 alone. Expression of a terminal adipose gene, FABP4, was not significantly different in all conditions (Figure 2D, bottom). With increased expression of UCP1 and other BAT-enriched genes upon overexpression of Dot1L and Zc3h10 (Figure 2D and 2E), we next assessed the functional consequence of the oxygen consumption. Indeed, forskolin-treated Dot1L alone overexpressing cells had somewhat increased OCR. Co-overexpression of both Dot1L and Zc3h10 further increased the total OCR as well as uncoupled OCR, suggesting cooperative function of Dot1L and Zc3h10 in browning of 3T3-L1 cells (Figure 2F). Altogether, these results demonstrate that Dot1L plays a critical role in promoting thermogenic program.

Figure 2. Dot1L promotes thermogenic gene program in vitro

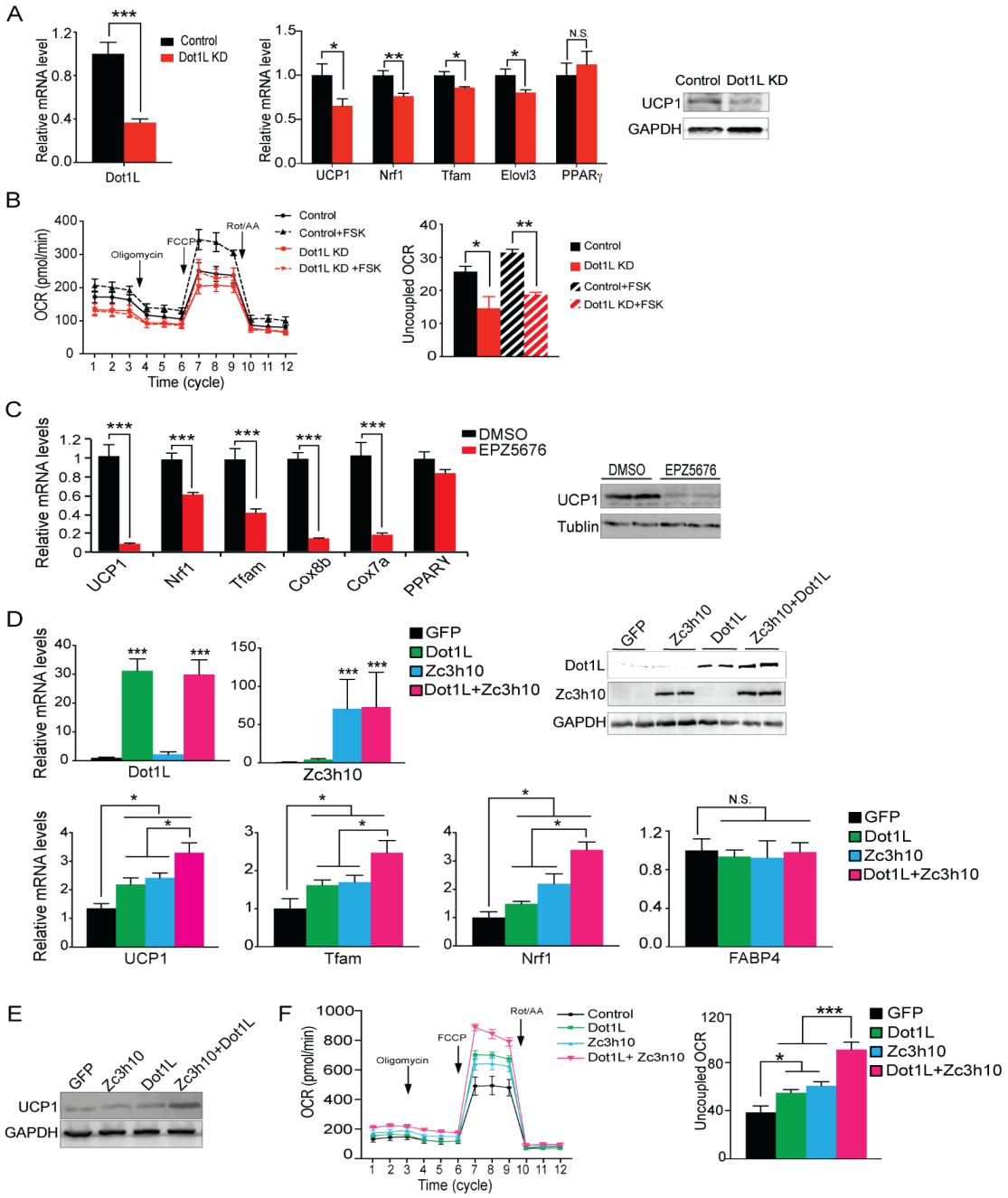

Figure 2. Dot1L promotes thermogenic gene program in vitro

(A) (Left) RT-qPCR for Dot1L and thermogenic genes in BAT cells infected either scrambled (Control) or adenovirus expressing short hairpin targeting Dot1L (Dot1L KD) after Day 2 of adipogenic differentiation. (Right) Immunoblotting for UCP1.

(B) (Left) OCR measured in Dot1L KD cells using Seahorse XF24 analyzer. (Right) Uncoupled OCR in BAT cells infected with control or shDot1L under oligomycin (0.5uM).

(C) (Left) RT-qPCR for indicated genes in SGC0496 treated BAT cells. BAT cells treated with either DMSO or Dot1L inhibitor EPZ5676 (5nM). (Right) Immunoblotting for UCP1.

(D) RT-qPCR for indicated genes and immunoblotting for indicated proteins in 3T3-L1 cells that were transduced with either AdGFP or AdZc3h10 or AdDot1L individually or in combination for

overexpression (OE) of Zc3h10 and Dot1L. The differentiated cells were treated with forskolin (10uM) for 6 hr to induce beiging.
(E) Immunoblotting for UCP1.
(F) (Left) OCR measured in Zc3h10 OE and Dot1L OE, individually and in combination in differentiated 3T3-L1 adipocytes that were induced to beiging. (Right) Uncoupled OCR under oligomycin (0.5 uM).

Inhibition of Dot1L activity impairs BAT gene program in vivo

To study Dot1L function in vivo, we first used a selective and potent small molecule inhibitor of Dot1L, EPZ5676. We administered either saline (control) or EPZ5676 to WT mice via daily subcutaneous injection for 8 days (Figure 3A). By immunoblotting with H3K79me3 antibody, we confirmed inhibition of H3K79 methylation in BAT of animals treated with EPZ5676 (Figure 3B, left). Indeed, BAT from the inhibitor treated mice showed significantly decreased mRNA levels for UCP1, Nrf1, and Tfam, as well as other thermogenic genes, such as PGC1α and Elovl3, while no changes in adipogenic transcription factor, such as PPARγ (Figure 3B, middle). Also, the immunoblotting detected significantly lower UCP1 protein levels in BAT of EPZ5676 treated mice compared to the control mice (Figure 3B, middle). Similarly, EPZ5676 treatment also decreased thermogenic gene expression in iWAT, WAT depot known to undergo browning (Figure 3B, right), but not in pWAT or in liver (Supplementary Figure 2A).

Next, to investigate the physiological outcome from decreased expression of thermogenic genes, we subjected these EPZ5676 treated mice to acute cold exposure at 4°C. Both groups of mice had body temperatures around 37°C prior to the cold exposure. After 4 hrs of cold exposure, the body temperature of the EPZ5676 treated mice was 4°C lower compared to their non-treated littermates, demonstrating the significantly reduced thermogenic capacity (Figure 3C). Next, we assessed the energy expenditure by measuring the whole body O_2 consumption using CLAMS. Indeed, EPZ5676 treated mice had significantly lower VO_2 than the control mice at 4°C (Figure 3D), whereas food intake and locomotive activity were similar between the two groups (Supplementary Figure 2B). Altogether, these results support that Dot1L enzymatic activity is critical for activating the thermogenic gene program in vivo.

Figure 3. Inhibition of Dot1L activity impairs BAT gene program in vivo

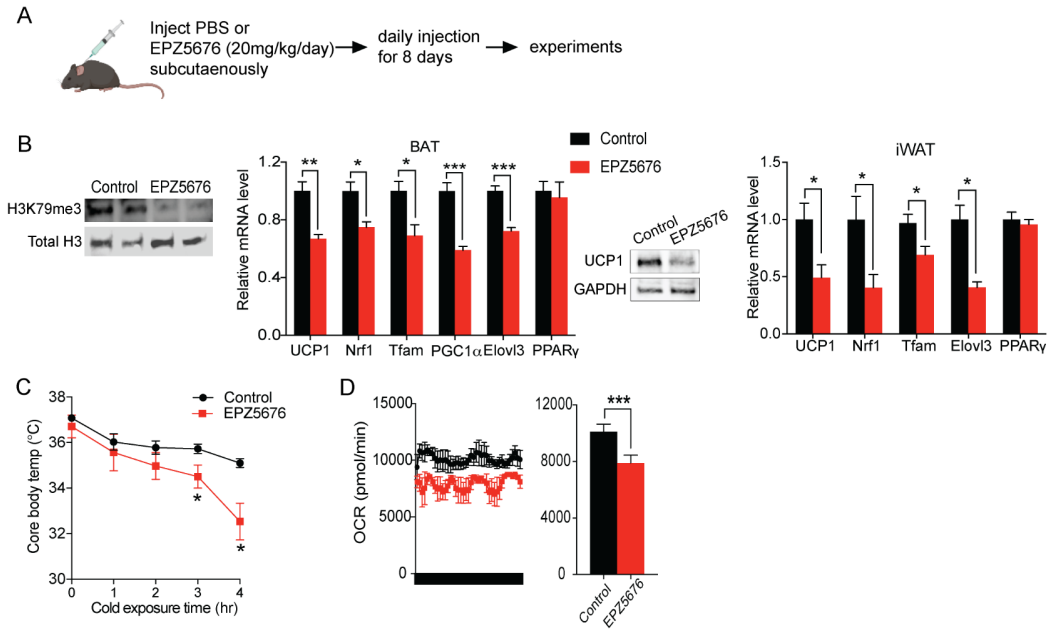

Figure 3. Inhibition of Dot1L activity impairs BAT gene program in vivo
(A) Schematic diagram of the strategy used to inject either Saline for control or Dot1L chemical inhibitor, EPZ5676.
(B) (Left) Immunoblotting for H3K79me3 and total H3. (Middle) RT-qPCR for indicated genes in BAT and iWAT from either PBS or EPZ5676 injected mice (n=4 mice per group) and immunoblotting for UCP1 protein.
(C) Rectal temperature of 14-wk old mice maintained at 4°C at indicated time points (hr) (n=4 mice per group)
(D) VO_2 assayed in mice that were housed at 4°C by indirect calorimetry using CLAMS.

Dot1L is required for cold-induced thermogenesis in mice

To further evaluate whether Dot1L is critical for the BAT gene program in vivo, we performed Dot1L ablation in $UCP1^+$ cells in mice (Dot1L-BKO) by crossing Dot1L floxed mice with UCP1-Cre mice (Figure 4A, left). We validated our mouse model by genotyping and by comparing Dot1L mRNA levels in BAT and iWAT of Dot1L-BKO mice and Dot1L f/f control mice (WT). Dot1L-BKO mice had a 70% reduction in Dot1L mRNA level in BAT. Dot1L-BKO mice also showed a 60% decrease in Dot1L mRNA level in iWAT, probably due to the mild cold exposure at room temperature that can induce $UCP1^+$ adipocytes in iWAT (Figure 4A, right). Importantly, UCP1 expression was significantly reduced by 40% and 60% in BAT and iWAT, respectively (Figure 4B). UCP1 protein level was reduced significantly, as detect in BAT (Figure 4B right). In addition, expression of other BAT enriched genes, such as Dio2 and CideA, and other Zc3h10 target genes, such as Tfam and Nrf1, were all significantly decreased in BAT and iWAT of Dot1L-BKO mice, compared to WT littermates (Figure 4C).

Dot1L is known to be the only known H3K79 methyltransferase (VanLeeuwen, 2002). Hence, we performed ChIP-qPCR, to assess methylation status of H3K79 methylation at the Zc3h10 binding region of the UCP1 promoter using BAT of mice. Indeed, we detected a 50% reduction in di-methylation and a 70% reduction in tri-methylation of H3K79 at the -4.6 kb UCP1 promoter region (Figure 4D). Thus, the decreased UCP1 mRNA level upon Dot1L ablation in BAT was correlated with decreased di-methylation and tri-methylation H3K79 at the UCP1 promoter region. Similar to the -4.6 kb UCP1 promoter region, H3K79 methylation status at the -200 bp Nrf1 promoter region and at the +50 bp Tfam region was also decreased (Figure 4D). We previous reported these regions to contain Zc3h10 binding sites. The reduced H3K79 methylation at Zc3h10 binding sites in BAT of Dot1L-BKO mice suggest that the recruitment of Dot1L by Zc3h10 to the target genes is important for BAT gene expression. Moreover, these observations support the notion that Dot1L participates in the transcriptional activation of UCP1 and other Zc3h0 target genes by modifying H3K9 methylation status.

To examine the effect of Dot1L deficiency on the thermogenic capacity, we subjected these Dot1L-BKO mice to an acute cold exposure at 4°C. While body temperatures of mice were similar initially, Dot1L-BKO mice were severely cold intolerant as their body temperature started to drop significantly after 2 hrs of cold challenge. After 3 hrs of cold exposure, the body temperature of Dot1L-BKO mice was 5°C lower than that of control mice (Figure 4E), an in vivo evidence of the requirement of Dot1L for cold-induced thermogenesis. Considering such lower thermogenic gene expression and decreased thermogenic capacity, we assessed the metabolic effect in the Dot1L-BKO mice by measuring whole body OCR using CLAMS. Indeed, the Dot1L-BKO mice had significantly reduced VO_2 compared to WT littermates at room temperature and at 4°C, while locomotor activity and food consumption were similar (Figure 4F and Supplementary Figure 3A). To examine the contribution of BAT to the altered energy expenditure in Dot1L-BKO mice, by Seahorse assay, we measured OCR in BAT dissected out from these mice. We found OCR in BAT from Dot1L-BKO mice to be decreased by 20%. (Figure 4F, right). In line with these results, we then asked whether decreased energy expenditure and impaired BAT function in Dot1L-BKO mice would be reflected in changes in

adiposity. The body weights of mice started to diverge starting on wk 10, then they were maintained on a high-fat-diet (HFD) from wk 11 to wk 13 of age. By 13 wks, the Dot1L-BKO mice were approximately 8 g heavier relative to the control mice (Figure 4G), and the Dot1L-BKO had significantly larger iWAT and pWAT depots, which primarily accounted for the higher total body weights of Dot1L-BKO mice (Supplementary Figure 3B). There were no differences in food/energy intake between the two genotypes despite differences in body weights. Collectively, these results establish a defective BAT function and impaired thermogenic capacity that affects adiposity in Dot1L-BKO mice and that Dot1L is required for the BAT thermogenic program in vivo.

Figure 4. Dot1L is required for cold-induced thermogenesis in mice

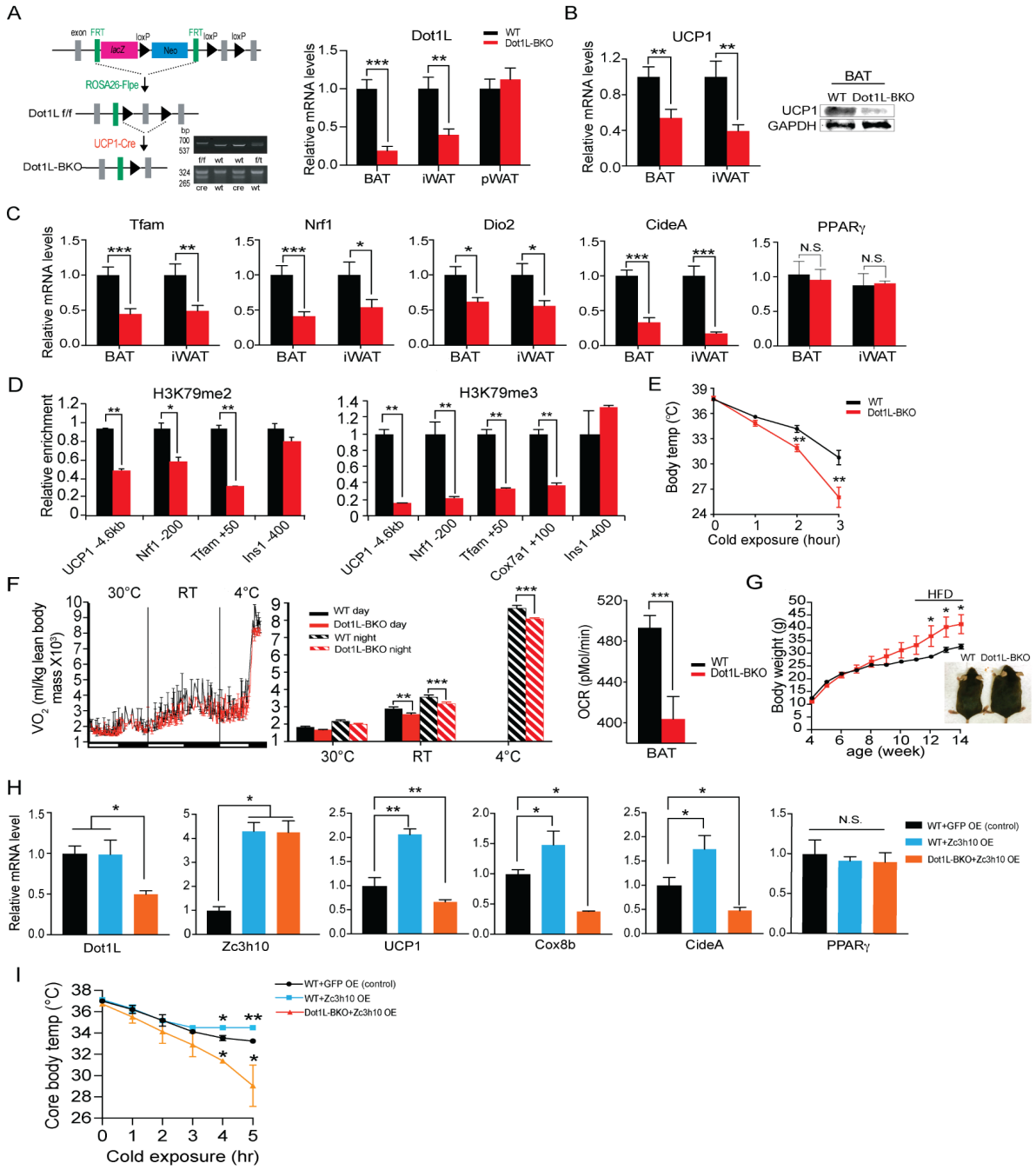

316 **Figure 4. Dot1L is required for cold-induced thermogenesis in mice**
317 **(A)** (Left) Schematic diagram of the strategy used to generate BAT specific Dot1L conditional
318 KO mice. PCR genotyping of the mice: Top gel, Dot1L allele; bottom gel, Cre. (Right) RT-qPCR
319 for Dot1L in BAT, iWAT and pWAT from Dot1L f/f (WT) and Dot1L-BKO mice (n=6 mice per
320 group).
321 **(B)** RT-qPCR and immunoblotting for UCP1 in BAT and iWAT from Dot1L f/f (WT) and Dot1L-
322 BKO mice.
323 **(C)** RT-qPCR for indicated genes in BAT and iWAT from Dot1L f/f (WT) and Dot1L-BKO mice.
324 **(D)** ChIP-qPCR of H3K79me2 and H3K79me3 at Zc3h10 binding regions of BAT tissue from
325 control (f/f) or Dot1L-BKO mice (n=5).
326 **(E)** Rectal temperature measured in 13 wk-old mice at 4°C at indicated time points (hours) (n=6
327 mice per group).
328 **(F)** (Left) whole body VO_2 assayed in WT and Dot1L-BKO mice, housed at indicated ambient
329 temperatures (n=6 per group) by indirect calorimetry using CLAMS. (Right) OCR measured in
330 BAT of WT and Dot1L-BKO mice using Seahorse XF24 Analyzer (n=5 per group).
331 **(G)** Representative photograph of 14 wk-old control and body weight of WT and Dot1L-BKO
332 mice fed HFD from wk 12.
333 **(H)** RT-qPCR for indicated genes from WT injected with GFP or Zc3h10 adenovirus or Dot1L-
334 BKO mice injected with Zc3h10 adenovirus for overexpression.
335 **(I)** Rectal temperature measured at 4°C at indicated time points (hours) (n=4 mice per group).
336
337 To test the relevance of Dot1L-Zc3h10 interaction to thermogenesis in vivo, we next
338 asked whether Dot1L is required for Zc3h10-induced thermogenesis. By direct injection of
339 Zc3h10 adenovirus into BAT, we overexpressed Zc3h10 in WT and in Dot1L-BKO mice. We
340 detected a 4-fold increase in Zc3h10 mRNA levels in BAT of Zc3h10 adenovirus-injected mice
341 (Zc3h10 OE). As expected, Dot1L-BKO mice showed a 60% reduction in Dot1L mRNA levels in
342 BAT (Figure 4H). We previously have reported that overexpression Zc3h10 in adipose tissue
343 enhances thermogenic gene expression (Yi et al., 2019). As predicted Zc3h10 overexpressing
344 mice had increased expression of BAT-enriched genes, such as UCP1, Cox8b, and CideA,
345 compared to the control mice. More importantly, expression BAT-enriched genes was
346 significantly reduced in Dot1L-BKO even upon Zc3h10 overexpression, while adipogenic
347 markers, such as PPARγ, remained unchanged (Figure 4H). These results show that Dot1L is
348 critical and required for activation of the thermogenic program by Zc3h10 in vivo. Moreover,
349 when these mice were subjected to cold exposure, Zc3h10 OE mice had higher core body
350 temperature compared to the control mice after 3 hrs (Figure 4I). However, Dot1L-BKO Zc3h10
351 OE mice were severely cold sensitive, and their body temperature was significantly lower than
352 the control and Zc3h10 OE mice. Collectively, these results demonstrate the requirement of
353 Dot1L-Zc3h10 interaction for activating the thermogenic program in brown fat.
354
355 **Dot1L increases chromatin accessibility for activation of thermogenic genes**
356 Thus far, we have shown that Dot1L-BKO mice have severely reduced thermogenic
357 capacity due to significantly decreased BAT gene expression accompanied with reduced
358 H3K79me2/3 at promoter regions of thermogenic genes. To study the underlying mechanism of
359 how Dot1L ablation in BAT decreases H3K79me2/3 to decrease chromatin accessibility, thereby
360 decreasing gene transcription, we used nuclei isolated from cold exposed Dot1L-BKO mice and
361 their littermates to assess the chromatin landscape during thermogenesis by Assay for
362 Transposase-Accessible Chromatin (ATAC-seq). Strikingly, Dot1L-BKO had significantly
363 reduced peaks genome wide near the transcription start sites (TSS), while WT had
364 concentrated open chromatin regions at TSS, as H3K79 methylation is reported as a gene
365 activation marker. (Fig 5A left). With our primary interest in assessing Dot1L's role in the
366 regulation of thermogenesis, we compared relative ATAC-seq peaks for thermogenic genes,

such as PRDM16, Zfp516, Cox8b and for mitochondria/oxidative phosphorylation, such as Cox7a1, Tfam, and Cyc1, in response to Dot1L ablation (Figure 5, middle). Also, Aifm2, Dot1L-BKO mice had much smaller peaks around promoters of UCP1, Cox8b and Elovl3 compared to WT mice (Figure 4, right), consistent with significantly decreased thermogenic gene expression in the Dot1L-BKO mice. Also, we found Dot1L-BKO had decreased expression of mitochondrial genes as well as Aifm2, a recently reported BAT-specific enzyme that converts NADH to NAD to sustain robust glycolysis to fuel thermogenesis (Nguyen et al., 2020). These data suggest that H3K79me2/3 by Dot1L is important for creating a chromatin landscape permissive to transcription in brown fat upon cold-stimulation.

Figure 5. Dot1L increases chromatin accessibility for activation of thermogenic genes

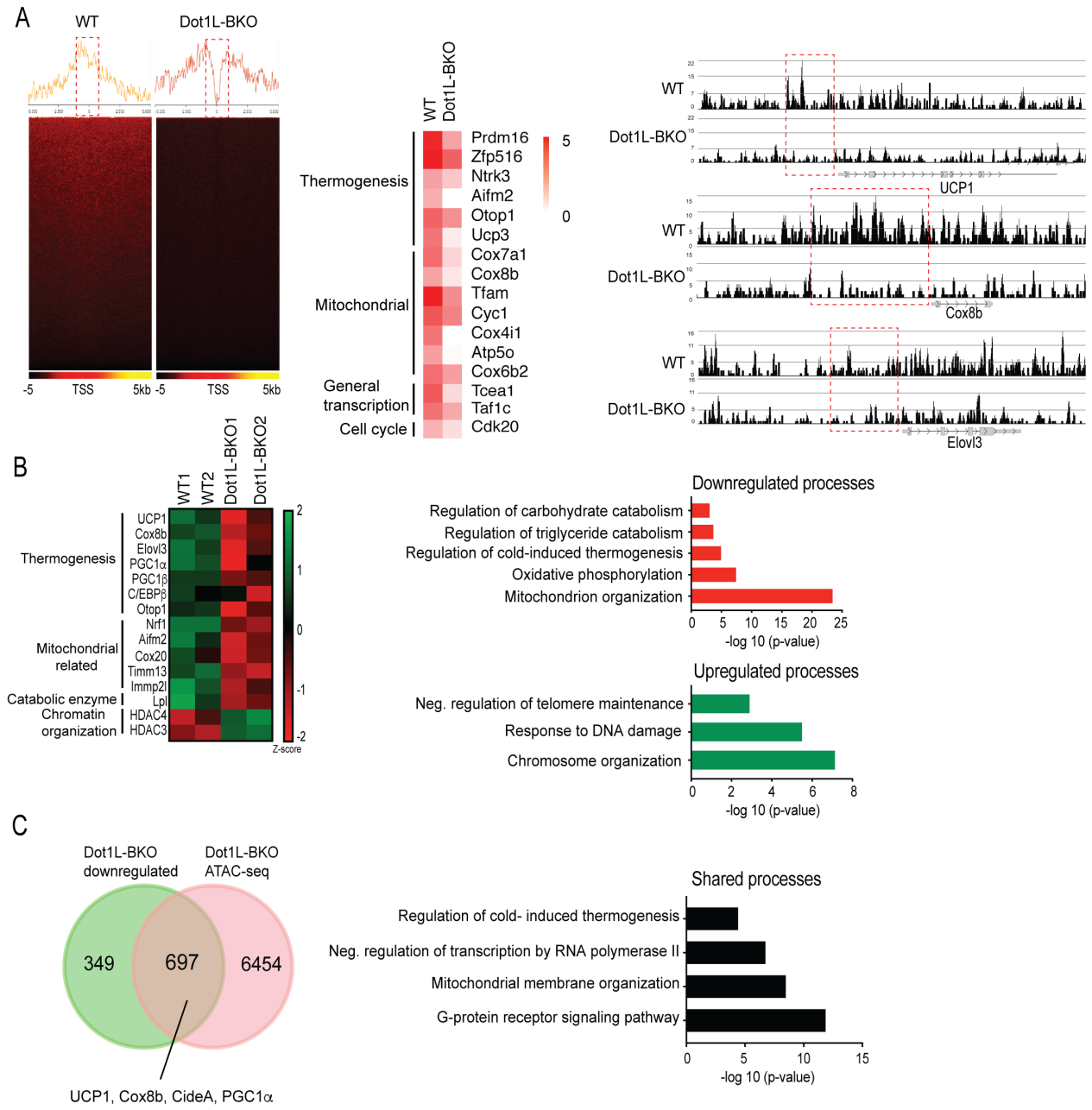

Figure 5. Dot1L increases chromatin accessibility for activation of thermogenic genes
(A) ATAC-seq using BAT from WT and Dot1L-BKO mice after 2 hr cold exposure n = 2 per group. (Left) Heatmaps showing open chromatin regions focused at the transcription start site (TSS). Color scale shows peaks detected. (Right) UCSC genome browser screenshot of representative peaks at a subset of promoter regions of thermogenic genes.
(B) RNA-seq using BAT from WT and Dot1L-BKO mice, n = 2 pooled RNA samples per group. (Left) Heatmap showing changes in gene expression. Color scale shows changes in gene expression as determined by Z-score, green is –2 and red is 2. (Middle) Representative top GO terms of upregulated and downregulated genes identified by differential expression analysis.
(C) Venn diagrams showing number of unique or shared genes between ATAC- and RNA-seq datasets and charts for representative top gene ontology (GO) terms.

Next, to examine gene expression changes upon Dot1L ablation in UCP1$^+$ cells as a result of chromatin compaction, we performed RNA-seq using BAT from Dot1L-BKO mice and their littermates. Gene ontology of genes that were at least 2-fold downregulated in Dot1L-BKO mice revealed that mitochondrion organization, oxidative phosphorylation and cold-induced thermogenesis were some of the most affected processes (Figure 5B, middle). Notably, the downregulated thermogenic genes include UCP1, Cox8b, Elov3 and PGC1α as well as those related to mitochondrion organization and oxidative phosphorylation such as Nrf1, Cox20, Tomm13, and Immp21 (Figure 5B, left). With ATAC-seq results, these data suggest a mechanistic link between Dot1L-mediated chromatin remodeling and the global landscape of genome accessibility in brown fat for thermogenic gene expression. In addition, regulation of triglyceride and carbohydrate catabolism were compromised by Dot1L ablation. Conversely, chromosome organization, negative regulation of telomere maintenance, response to DNA damage were upregulated in the Dot1L knockout. In fact, we detected upregulated genes involved in chromatin compaction and gene repression, such as HDAC3, HDAC4 and DNMT1, further supporting that Dot1L increases chromatin accessibility (Figure 5B, right).

We then compared RNA-seq data to ATAC-seq obtained to identify common downregulated pathways found at lower levels using ATACs upon Dot1L ablation in UCP1+ cells, and we found about 40% of the total of downregulated genes were also detected from the ATAC-seq dataset (Figure 5C, left). Some of similar processes between the two datasets include regulation of cold-induced thermogenesis, transcription initiation/elongation factors, mitochondrial membrane organization as well as G-protein receptor signaling pathway (Figure 5C, right). Remarkably, the cluster of shared genes included thermogenic genes, such *as* UCP1*,* PGC1α*,* Cox8b, CideA*,* further underscoring the importance of Dot1L in brown adipose tissue. This suggest that Dot1L ablation results in reduced chromatin accessibility, leading to downregulated gene expression for those specific pathways. Altogether, we conclude that H3K79me2/3 by Dot1L plays a critical role in the activation of transcription of thermogenic genes by increasing chromatin accessibility.

DISCUSSION

Numerous studies have supported the concept that a network of transcription factors and epigenetic coregulators must work together to fine-tune thermogenic program in response to environmental conditions (Sambeat et al., 2017). Here, we identify Dot1L, the only known H3K79 methyltransferase, as an interacting partner of Zc3h10, a transcriptional factor that activates UCP1, as well as Tfam and Nrf1, for thermogenesis. We show that Dot1L is recruited by Zc3h10 to the UCP1 and other thermogenic genes. We demonstrate that Dot1L directly interacts with Zc3h10 to co-occupy the same region of the UCP1 promoter. Zc3h10 binds to Dot1L via the 501-1000aa fragment, which is largely composed of coiled coil domains,

428 evolutionarily conserved and widely-known for protein-protein interactions (Mier et al., 2017).
429 This same coiled coil domain has been reported to interact with some of mixed lineage leukemia
430 (MLL) oncogenic fusion proteins, such as AF10, to induce H3K79 methylation and constitutively
431 activate a leukemic transcriptional program (Song et al., 2019). Here, we show that Dot1L is
432 required for Zc3h10's function for thermogenic gene program. In fact, Zc3h10 overexpression
433 could not rescue the decreased thermogenic gene expression upon Dot1L ablation in mice,
434 demonstrating that Dot1L is critical in Zc3h10 mediated activation of thermogenesis.
435 We establish that H3K79me2/3, catalyzed by Dot1L, as an activation mark for
436 thermogenic gene program. In this regard, previous studies reported that H3K79 methylation is
437 strongly associated with active transcription (Steger et al., 2008, Wood et al., 2018). Our Dot1L-
438 BKO mice showed a markedly less open chromatin regions in promoter regions of thermogenic
439 genes. The ATAC-seq data showed significantly reduced peaks genome-wide near the
440 transcription start sites (TSS) in BAT of Dot1L-BKO mice, compared to control mice that had
441 concentrated open chromatin regions at TSS upon cold exposure. In addition, studies reported
442 that H3K79me2/3 may be active enhancer marks and may even be required for enhancer-
443 promoter interactions to increase transcription (Markenscoff-Papadimitriou et al., 2014, Gilan et
444 al., 2016, Godfrey et al., 2019). Godfrey et al. found H3K79me2/3 to be abundant at a subset of
445 super-enhancers in MLL-related leukemia cells and that a loss of H3K79me2/3 by Dot1L
446 inhibition led to significantly reduced enhancer-promoter interaction coupled with a decrease in
447 transcription (Godfrey et al., 2019). We show that Dot1L is recruited by Zc3h10 to a UCP1
448 upstream region of -4.6 kb, a region suggested to be one of so-called super enhancers (SEs)
449 (Whyte et al., 2013; Harms et al., 2015). In fact, Dot1L ablation in BAT of mice resulted in a
450 significantly reduction of H3K79me2/3 at the -4.6 kb UCP1 region, correlating with decreased
451 expression of UCP1. It is possible that H3K79me2/3 catalyzed by Dot1L may be important in
452 maintaining enhancer/promoter association for transcriptional activation.
453 Due to limited accessibility of the H3K79 residue, located in the nucleosome core, how
454 H3K79 methylation promotes gene activation is not clearly understood (van Leeuwen et al.,
455 2002, Lu et al., 2008). Several studies support the concept that H3K79me2/3 and other well-
456 profiled gene activation marks are interdependent (Steger et al., 2008). Steger et al.
457 demonstrated that H3K79me2/3 at gene promoters highly correlates with H3K4me1/2/3 and
458 H3K36me3, known gene activation marks in mammalian cells. Furthermore, Chen et al.
459 reported that Dot1L may inhibit the localization of SIRT1 and SUV39H1, a H3K9ac demethylase
460 and a H3K9me2 methyltransferase, respectively, at MLL fusion target genes correlating with
461 elevated H3K9ac and low H3K9me2, to maintain an open chromatin state (Chen et al., 2015).
462 These authors proposed that H3K79me2/3 mark, in part, may function by inhibiting the histone
463 deacetylase activity (Chen et al., 2015, Kang et al., 2018). In line with these findings, Dot1L
464 probably works with other histone modifiers to maintain activation marks or to suppress
465 repressive marks. Regardless, we establish that H3K79me2 and H3K79me3, in particular,
466 function as activation marks for thermogenic gene program.
467 Overall, we demonstrate that Dot1L is critical for thermogenic program and is required
468 for Zc3h10-induced thermogenesis through its H3K79 methyltransferase activity. With combined
469 ATAC-seq and RNA-seq data, we provide molecular evidence that the decreased thermogenic
470 gene expression is due to decreased H3K79me2/3 on promoter regions of thermogenic genes,
471 as well as genes involved in chromatin remodeling. Consequently, our mouse line with Dot1L
472 ablated in UCP1^{+} cells had significantly decreased thermogenic gene expression including
473 UCP1, resulting in cold intolerance with decreased oxygen consumption (Figure 4C-E), leading
474 to increased adiposity.
475
476 **MATERIALS AND METHODS**
477
478 **Animals**

479 Dot1L conditional knock-out mice (Dot1ltm1a(KOMP)Wtsi) for this research project were
480 generated by the trans-NIH Knock-Out Mouse Project (KOMP) and obtained from the KOMP
481 Repository (www.komp.org). NIH grants to Velocigene at Regeneron Inc (U01HG004085) and
482 the CSD Consortium (U01HG004080) funded the generation of gene-targeted ES cells for 8500
483 genes in the KOMP Program and archived and distributed by the KOMP Repository at UC Davis
484 and CHORI (U42RR024244). Mice were first mated with FLPe mice from Jackson Lab. FLP
485 mediated recombination was confirmed by PCR and resultant progeny were mated with UCP1-
486 cre mice (B6.FVB-Tg(Ucp1-cre)1Evdr/J) also from Jackson Lab.Unless otherwise stated, mice
487 used in experiments were male and between 10 -14 weeks of age. Mice were fed a chow diet or
488 a palatable high fat diet (45% fat derived calories- Dyets) ad libitum. EPZ-5676 was purchased
489 from MedChemExpress (Cat. No.: HY-15593) and injected 20mg/kg/day for 8 days into BAT. All
490 protocols for mice studies were approved from the University of California at Berkeley Animal
491 Care and Use Committee.
492
493 **GST-pulldown**
494 GST-Dot1L was purchased from epicypher. GST and GST-Dot1L plasmids were
495 transformed into BL21(DE3) E. coli (NEB) and production was induced by induction by 0.1M
496 IPTG. Resultant proteins were purified using Glutathione Sepharose 4B (GE) according to the
497 manufacturer recommended protocol. [35S]-labeled Zc3h10 protein was produced by using TNT
498 coupled transcription/translation kit (Promega). 20ug of GST fusion proteins were incubated for
499 2hrs at 4°C with in vitro translated Zc3h10 and glutathione sepharose beads. The beads were
500 washed 3 times with binding buffer, and bound proteins were eluted by boiling in Laemmli
501 sample buffer, separated by SDS-PAGE and analyzed by autoradiography.
502
503 **TAP assay and mass spectrometry Analysis**
504 10ug of Zc3h10-CTAP or CTAP vector plasmid were transfected in 293FT cells using
505 lipofectamine 2000 (Invitrogen). Cells were lysed and IPed using buffers from the InterPlay
506 Mammalian TAP system manufacturer recommended with the noted exception: after binding of
507 the cell lysates to the Streptavidin resin, the resin was re-incubated with 200ug of BAT nuclear
508 extracts diluted to 1mL in SBB overnight. TAP eluates were boiled in SDS, ran on an SDS-
509 PAGE gel, and stained with Coomassie Brilliant Blue (Sigma). Bands that were identified to be
510 specific to the Zc3h10-TAP lane were excised from both the Zc3h10-TAP and TAP vector lanes
511 and protein were identified by mass spectrometry performed by the Vincent J. Coates
512 Proteomics/ Mass Spectrometry Laboratory (P/MSL) at UC Berkeley.
513
514 **Cold-induced Thermogenesis**
515 Core body temperature was determined using a Physitemp BAT-12 probe at 4°C.
516
517 **Indirect Calorimetry**
518 Oxygen Consumption was measured using the Comprehensive Laboratory Animal
519 Monitoring System (CLAMS). Data were normalized to lean body mass determined by
520 EchoMRI. Mice were individually caged and maintained under a 12 hr light/12 hr dark cycle.
521 Food consumption and locomotor activity were tracked.
522
523 **Cell culture**
524 HEK293FT and 3T3-L1 cell lines were obtained from UCB Cell Culture Facility which is
525 supported by The University of California Berkeley. The immortalized BAT cell line was from Dr.
526 Shingo Kajimura (Harvard). Cells were grown in standard condition with 5% CO2, at 37°C. BAT
527 cells, 3T3-L1 and 293FT cells were maintained in DMEM containing 10% FBS and 1%
528 pen/strep prior to differentiation/ transfection. Brown adipocyte differentiation was performed as
529 described in (Yi et al., 2019). Ad-m-Dot1L-shRNA, Ad-Zc3h10-flag adenovirus and Ad-GFP-m-

530 DOT1L were purchased from Vector Biolabs. Knockdown of Dot1L accomplished using
531 adenoviral transduction of MOI of 250 at day 4 of brown adipocyte differentiation. Differentiation
532 of 3T3-L1 was induced by treating confluent cells with DMEM containing 10% FBS, 850nM
533 insulin, 0.5mM isobutyl-methylxanthine, 1μM dexamethasone, 1nM T3, 125 nM indomethacin.
534 After 48h of induction, cells were switched to a maintenance medium containing 10% FBS,
535 850nM insulin, 1nM T3. 3T3-L1 cells were infected on day 4 of differentiation using either GFP,
536 Dot1L or Zc3h10 adenoviruses. Then, viral medium was replaced by maintenance medium the
537 following day. To stimulate thermogenesis, differentiated 3T3-L1 cells were treated 6h with
538 10μM forskolin on day 6. Inhibition of Dot1l was accomplished by addition of either 5nM
539 EPZ5676 (MedChemExpress, Cat. No.: HY-15593) or DMSO.
540
541 **Seahorse oxygen consumption assay**
542 BAT cell line cells were differentiated in 12-well plates, trysinized, and reseeded in XF24
543 plates at 50K cells per well at day 4 of differentiation and assayed on day 5 of differentiation. On
544 the day of experiments, the cells were washed three times and maintained in XF-DMEM
545 (Sigma-Aldrich) supplemented with 1 mM sodium pyruvate and 17.5 mM glucose. Oxygen
546 consumption was blocked by 1 μM oligomycin. Maximal respiratory capacity was assayed by
547 the addition of 1 μM FCCP. Tissues were incubated for 1 hour at 37°C without CO_2 prior to
548 analysis on the XF24 Analyzer. Uncoupled respiration was calculated as OCR under oligomycin
549 treatment minus OCR under antimycin A/rotenone.
550
551 **RT-qPCR Analysis and Western blotting**
552 Reverse transcription was performed with 500ng of total RNA using SuperScript III
553 (Invitrogen). RT-qPCR was performed in triplicate with an ABI PRISM 7500 sequence detection
554 system (Applied Biosystems) to quantify the relative mRNA levels for various genes. Statistical
555 analysis of the qPCR was obtained using the ΔΔCt (2^-ddCT) method with Eef1a1 or 18s as the
556 control. RT-qPCR primer sets are listed in Table 1. Library generation for RNA sequencing was
557 carried out at the Functional Genomics Laboratory at UC Berkeley.
558 For western blot analysis, total cell lysates were prepared using RIPA buffer and nuclear
559 extracts were isolated using the NE-PER Nuclear and Cytoplasmic Extraction kit (Thermo).
560 Proteins were separated by SDS-PAGE, transferred to nitrocellulose membrane and probed
561 with the indicated antibodies.
562
563 **Antibodies**
564 The following antibodies were used where indicated: UCP1 (Abcam, 10983), Zc3h10
565 (Thermo Fisher, PA5-31814; for immunoblotting), Zc3h10 (Abnova, H00084872-B01P; for
566 ChIP), GAPDH (Cell signaling, 5174S), Dot1L (Bethyl, A300-953A), FLAG (Cell signaling,
567 14793S), HA (Cell signaling, 3724S), Tubulin (Abcam, Ab52866), Histone H3 (Cell signaling,
568 4499S), H3K79me3 (Abcam, ab2621), H3K79me2 (Abcam, ab3594)
569
570 **Luciferase-reporter Assay**
571 293FT cells were transfected with 300ng Zc3h10 and/or Dot1L, together with 100 ng of
572 indicated luciferase reporter construct and 0.5ng pRL-CMV in 24-well plates. Cells were lysed
573 48h post-transfection and assayed for luciferase activity using the Dual-Luciferase Kit
574 (Promega) according to manufacturer recommended protocol.
575
576 **Plasmid Constructs**
577 The HA-Dot1L expression vector was purchased from Genecopeiea. The Dot1L
578 sequence was subcloned by PCR amplifying and inserting into CTAP vectors from Agilent as
579 well as pGEX-4T-3 from GE.
580

581 **Coimmunoprecipitation**
582 For Co-IP experiments using tagged constructs, 293FT cells were transfected using
583 Lipofectamine2000 to express FLAG-tagged Zc3h10 and HA-tagged Dot1L. Cells were lysed in
584 IP buffer containing 20 mM Tris, pH 7.4, 150 mM NaCl, 1mM EDTA, 10% glycerol, 1% NP-40
585 supplemented with proteases inhibitors. Total cell lysates were incubated 2 hours at 4°C with
586 either anti-FLAG M2. For Co-IP in brown adipose tissue of wild type mice, nuclear extraction
587 was carried out using the NE-PER Nuclear and Cytoplasmic Extraction kit (Thermo). Equal
588 amounts of nuclear extracts were incubated with specific antibodies and protein A/G agarose
589 beads overnight at 4°C. Agarose beads were washed 3 times and bound proteins were eluted
590 by boiling in Laemmli sample buffer and analysed by immunoblotting using the indicated
591 antibodies.
592
593 **ChIP-qPCR**
594 ChIP was performed using ChIP kit (Cell signaling, 57976s). Briefly, BAT cells
595 overexpressing Dot1L or Zc3h10 were fixed with disuccinimidyl glutarate (DSG) at 2 mM
596 concentration in PBS for 45 min at room temperature before cross-linking with 1% methanol-free
597 formaldehyde in PBS for 10 min. For ChIP experiments in BAT, tissues from 3 BATs were
598 combined and minced on ice. The reaction was stopped by incubating with 125 mM glycine for
599 10 min. Cells or tissues were rinsed with ice-cold phosphate-buffered saline (PBS) for three
600 times, and lysed in IP lysis buffer containing 500 mM HEPES-KOH, pH 8, 1 mM EDTA, 0.5 mM
601 EGTA, 140 mM NaCl, 0.5% NP-40, 0.25% Triton X-100, 10% glycerol, and protease inhibitors
602 for 10 min at 4 °C. Nuclei were collected by centrifugation at 600 × g for 5 min at 4 °C. Nuclei
603 were released by douncing on ice and collected by centrifugation. Nuclei were then lysed in
604 nuclei lysis buffer containing 50 mM Tris, pH 8.0, 1% SDS 10 mM EDTA supplemented with
605 protease inhibitors, and sonicated three times by 20 s burst, each followed by 1 min cooling on
606 ice. Chromatin samples were diluted 1:10 with the dilution buffer containing 16.7 mM Tris pH
607 8.1, 0.01% SDS 1.1 % Triton X-100 1.2 mM EDTA, 1.67 mM NaCl, and proteinase inhibitor
608 cocktail. Soluble chromatin was quantified by absorbance at 260 nm, and equivalent amounts of
609 input DNA were immunoprecipitated using 10 µg of indicated antibodies or normal mouse IgG
610 (Santa Cruz) and protein A/G magnetic beads (Thermo-Fisher). After the beads were washed
611 and cross-linking reversed, DNA fragments were purified using the Simple ChIP kit (cell
612 signaling). Samples were analyzed by qPCR using the primer sets in Table 1 for enrichment in
613 target areas. The promoter occupancy for UCP1 and other indicated genes was confirmed by
614 RT-qPCR. The fold enrichment values were normalized to input.
615
616 **RNA-seq**
617 WT and Dot1L-BKO mice were cold exposed for 2 hr. Total RNA from BAT was
618 prepared using RNEasy kit (Qiagen). Strand-specific libraries were generated from 500 ng total
619 RNA using the TruSeq Stranded Total RNA Library Prep Kit (Illumina). cDNA libraries were
620 single-end sequenced (50 bp) on an Illumina HiSeq 2000 or 4000. Using Partek software, reads
621 were aligned to the mouse genome (NCBI38/mm10). A gene was included in the analysis if it
622 met all the following criteria: the maximum RPKM reached four at any time point, the gene
623 length was >100 bp. Selected genes were induced at least +/- 1.8-fold, and the expression was
624 significantly different from the basal ($p<0.05$).
625
626 **ATAC-seq**
627 For ATAC-seq, we used two mice per condition and processed nuclei extracted from
628 BAT separately, thus each sample analyzed was a separate biological replicate. ATAC-seq was
629 performed using Nextera DNA library Preparation kit (Illumina, 15028212) according to Chen et
630 al. 50. In all, 5×10^4 nuclei from tissues were collected in lysis buffer containing 10 mM Tris pH
631 7.4, 10 mM NaCl, 3 mM MgCl2, and 1% NP-40, and spun at 500 × g at 4 °C for 10 min. The

632 pellets were resuspended in the transposase reaction mixture containing 25 μL
633 2 × Tagmentation buffer, 2.5 μL transposase, and 22.5 μL nuclease-free water, and incubated at
634 37 °C for 30 min. The samples were purified using MinElute PCR Purification kit (Qiagen,
635 28006) and amplification was performed in 1 × next PCR master mix (NEB, M0541S) and
636 1.25 μM of custom Nextera PCR primers 1 and 2 with the following PCR conditions: 72 °C for
637 5 min; 98 °C for 30 s; and thermocycling at 98 °C for 10 s, 63 °C for 30 s, and 72 °C for 1 min.
638 Samples were amplified for five cycles and 5 μL of the PCR reaction was used to determine the
639 required cycles of amplification by qPCR. The remaining 45 μL reaction was amplified with the
640 determined cycles and purified with MinElute PCR Purification kit (Qiagen, 28006) yielding a
641 final library concentration of ~30 nM in 20 μL. Libraries were subjected to pair-end 50 bp
642 sequencing on HiSeq4000 with 4–6 indexed libraries per lane. Partek Flow Genomics Suite was
643 used to analyze sequencing data. Reads were aligned to mm10 genome assembly using BWA-
644 backtrack. MACS2 in ATAC mode was then used to identify peaks from the aligned reads with a
645 q-value cutoff of 0.05 and fold enrichment cutoff of 2.0. Quantify regions tool was used to
646 quantify the peaks identified by MACS2 from each sample to generate a union set of regions.
647 Regions were then annotated to RefSeq mRNA database and analysis of variance (ANOVA)
648 was performed to determine significant peak differences between groups. UCSC genome
649 browser was used to visualize peaks. Gene set enrichment and pathway analysis was used to
650 highlight biological processes with the highest q-values among those identified.
651
652 **Statistical analysis**
653 Statistical comparisons were made using a two-tailed unpaired t-test using GraphPad
654 Prism 8 software (GraphPad Software Inc., La Jolla, CA, USA). For genome-wide analyses, we
655 employed Partek Genomics Suite (Partek Inc., St. Louis, Missouri, USA) using ANOVA for
656 ATAC-seq comparisons, and DESeq2 for RNA-seq differential expression comparisons, and
657 subsequently used Gene set enrichment tool for gene ontology to identify the significantly
658 affected pathways presented in Data are expressed as means ± standard errors of the means
659 (SEM). The statistical differences in mean values were assessed by Student's *t* test. All
660 experiments were performed at least twice and representative data are shown.
661
662 **AUTHOR CONTRIBUTIONS**
663
664 D.Y. performed loss-of-function/gain-of-function studies in vitro/in vivo experiments.
665 H.P.N. performed the interaction studies and assisted in animal studies. J.D. assisted in animal
666 studies. J.V. made plasmid constructs and performed bioinformatics analysis and edited the
667 manuscript. Y.X. assisted in RT-qPCR/immunoblotting. J.M.D. found and characterized Dot1L.
668 Y.W. performed ChIP and ATAC-seq. H.S.S. designed the project and guided experiments.
669 D.Y., H.P.N., and H.S.S wrote the manuscript.
670
671 **ACKLOWLDGEMENTS**
672
673 We thank M. Zhu for technical assistance. The work was supported by NIH grant
674 DK120075 to H.S.S.
675
676 **COMPETING INTERESTS**
677
678 The authors declare no competing interests.
679
680 **SUPPLEMTARY FIGURES AND TABLES**
681

S1. Dot1L directly interacts with Zc3h10 for UCP1 promoter activation

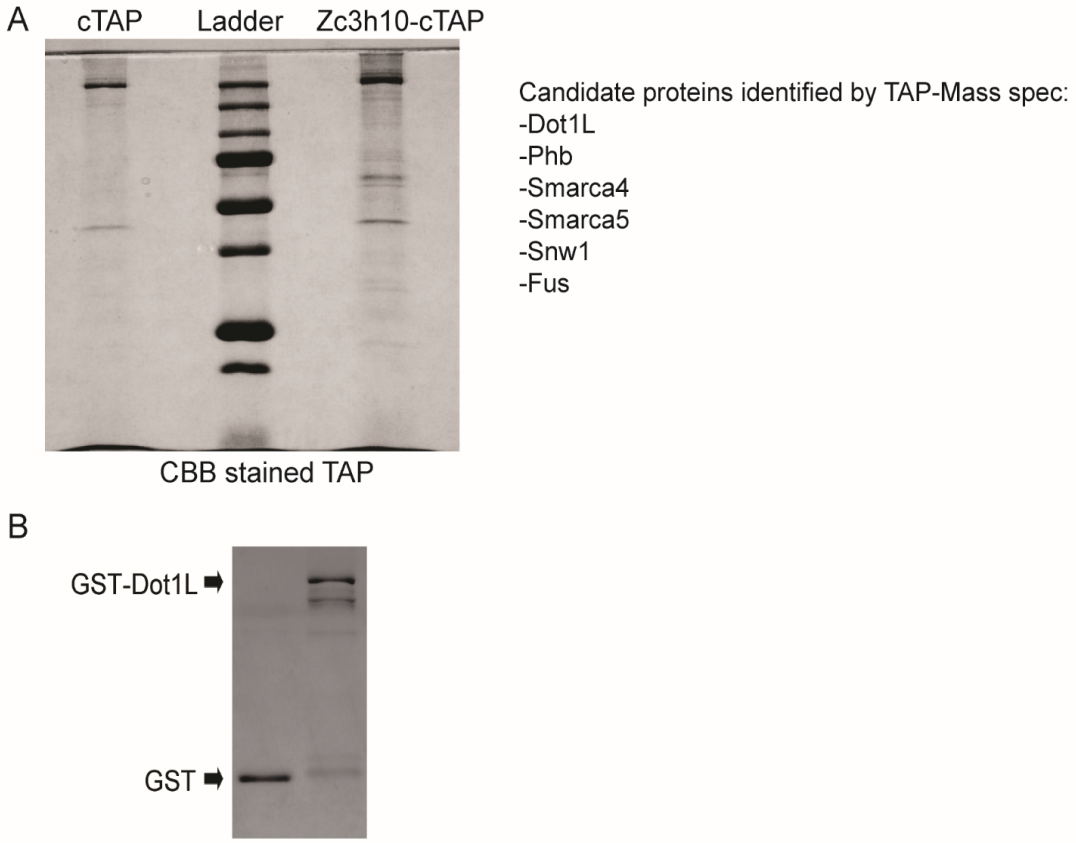

(A) Gel stained with Coomassie Blue after cTAP purification assay and a list of potential Zc3h10 interacting proteins identified by Mass spec

(B) Coomassie staining for GST alone and GST-Dot1L fusion protein

682

S2. Inhibition of Dot1L activity impairs BAT gene program in vivo

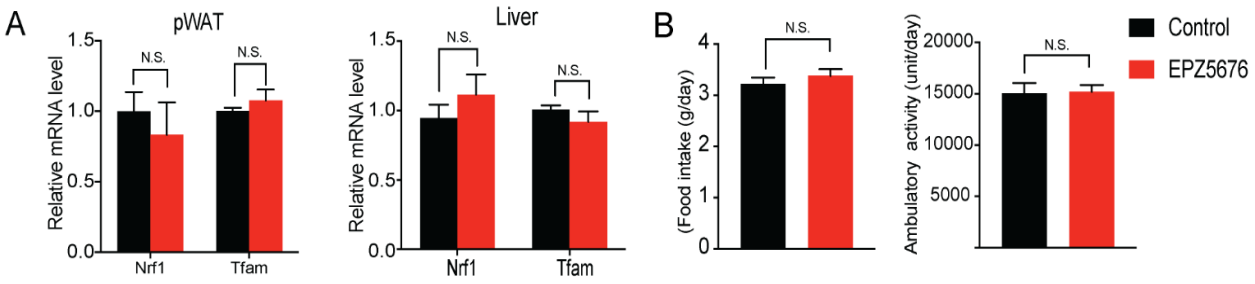

(A) RT-qPCR for indicated genes in pWAT and liver of control and EPZ5676 injected mice.
(B) Food intake and locomotor activity of control and EPZ5676 injected mice.

683

S3.Dot1L is required for cold-induced thermogenesis in mice

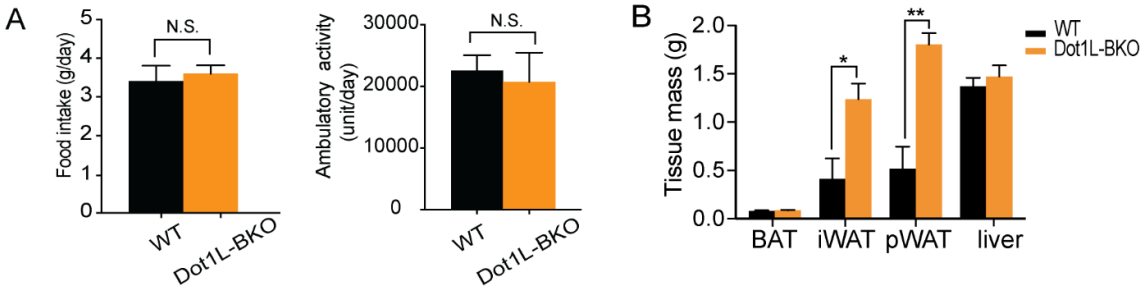

(A) Food intake and locomotor activity of WT and Dot1L-BKO mice.
(B) Body weight and mass of various tissues taken from WT and Dot1L-BKO mice at 14-week of age.

Table 1: Primer Sets used for RT-qPCR

	Forward Primer	Reverse Primer
Dot1L	CGA CTA ATG CTG CAC CTC CT	AGG AGT AGT GGT GTG GCT CA
UCP1	ACT GCC ACA CCT CCA GTC ATT	CTT TGC CTC ACT CAG GAT TGG
Tfam	GTC CAT AGG CAC CGT ATT GC	CCC ATG CTG GAA AAA CAC TT
Zc3h10	CGA CTA ATG CTG CAC CTC CT	AGG AGT AGT GGT GTG GCT CA
Nrf1	GAC AAG ATC ATC AAC CTG CCT GTA G	GCT CAC TTC CTC CGG TCC TTT G
Cox8b	TGT GGG GAT CTC AGC CAT AGT	AGT GGG CTA AGA CCC ATC CTG
Cox7a1	CAG CGT CAT GGT CAG TCT GT	AGA AAA CCG TGT GGC AGA GA
Eef1a1	ACG AGG CAA TGT TGC TGG TGA C	GTG TGA CAA TCC AGA ACA GGA GC
Elovl3	TCC GCG TTC TCA TGT AGG TCT	GGA CCT GAT GCA ACC CTA TGA
PGC1α	CCC TGC CAT TGT TAA GAC C	TGC TGC TGT TCC TGT TTT C
PPARγ	GTG CCA GTT TCG ATC CGT AGA	GGC CAG CAT CGT GTA GAT GA
CideA	TGC TCT TCT GTA TCG CCC AGT	GCC GTG TTA AGG AAT CTG CTG
Dio2	CAG TGT GGT GCA CGT CTC CAA TC	TGA ACC AAA GTT GAC CAC CAG
FABP4	ACA CCG AGA TTT CCT TCA AAC TG	CCA TCT AGG GTT ATG ATG CTC TTC A
Pdgfrα	CAAACCCTGAGACCACAATG	TCCCCCAACAGTAACCCAAG
UCP1-4.6kb	CTC AGA GTG CAA CCC CTC AC	GAG GTC GCA GAT CTG TTC CA

Nrf1 -200	GGT CCA ATC AGA TAG CCG GG	CCT CAC TCA TTG GTG GGT CC
Tfam +50	CTC GGG CCG ACG AAT GAT G	CGG GCT TCC CAC AGT ACC C
Ins1 -400	TGA CCA ATG AGT GGG CTA CG	CCA TTG ATA GCT GGG CCC TT

686
687
688 **REFERENCES**
689

690 CANNON, B. & NEDERGAARD, J. 2004. Brown adipose tissue: function and physiological
691 significance. *Physiol Rev,* 84**,** 277-359.
692 CHEN, C. W., KOCHE, R. P., SINHA, A. U., DESHPANDE, A. J., ZHU, N., ENG, R., DOENCH, J. G., XU,
693 H., CHU, S. H., QI, J., WANG, X., DELANEY, C., BERNT, K. M., ROOT, D. E., HAHN, W. C.,
694 BRADNER, J. E. & ARMSTRONG, S. A. 2015. DOT1L inhibits SIRT1-mediated epigenetic
695 silencing to maintain leukemic gene expression in MLL-rearranged leukemia. *Nat Med,*
696 21**,** 335-43.
697 CHONDRONIKOLA, M., VOLPI, E., BORSHEIM, E., PORTER, C., ANNAMALAI, P., ENERBACK, S.,
698 LIDELL, M. E., SARAF, M. K., LABBE, S. M., HURREN, N. M., YFANTI, C., CHAO, T.,
699 ANDERSEN, C. R., CESANI, F., HAWKINS, H. & SIDOSSIS, L. S. 2014. Brown adipose tissue
700 improves whole-body glucose homeostasis and insulin sensitivity in humans. *Diabetes,*
701 63**,** 4089-99.
702 CYPESS, A. M., LEHMAN, S., WILLIAMS, G., TAL, I., RODMAN, D., GOLDFINE, A. B., KUO, F. C.,
703 PALMER, E. L., TSENG, Y., DORIA, A., KOLODNY, G. M. & KAHN, C. R. 2009. Identification
704 and Importance of Brown Adipose Tissue in Adult Humans. *New England Journal of*
705 *Medicine,* 360**,** 1509-1517.
706 DEMPERSMIER, J., SAMBEAT, A., GULYAEVA, O., PAUL, S. M., HUDAK, C. S., RAPOSO, H. F.,
707 KWAN, H. Y., KANG, C., WONG, R. H. & SUL, H. S. 2015. Cold-inducible Zfp516 activates
708 UCP1 transcription to promote browning of white fat and development of brown fat.
709 *Mol Cell,* 57**,** 235-46.
710 FARMER, S. R. 2008. Molecular determinants of brown adipocyte formation and function.
711 *Genes Dev,* 22**,** 1269-75.
712 FENG, Q., WANG, H., NG, H. H., ERDJUMENT-BROMAGE, H., TEMPST, P., STRUHL, K. & ZHANG,
713 Y. 2002. Methylation of H3-lysine 79 is mediated by a new family of HMTases without a
714 SET domain. *Curr Biol,* 12**,** 1052-8.
715 FREDERIKS, F., TZOUROS, M., OUDGENOEG, G., VAN WELSEM, T., FORNEROD, M., KRIJGSVELD,
716 J. & VAN LEEUWEN, F. 2008. Nonprocessive methylation by Dot1 leads to functional
717 redundancy of histone H3K79 methylation states. *Nat Struct Mol Biol,* 15**,** 550-7.
718 GILAN, O., LAM, E. Y., BECHER, I., LUGO, D., CANNIZZARO, E., JOBERTY, G., WARD, A., WIESE,
719 M., FONG, C. Y., FTOUNI, S., TYLER, D., STANLEY, K., MACPHERSON, L., WENG, C. F.,
720 CHAN, Y. C., GHISI, M., SMIL, D., CARPENTER, C., BROWN, P., GARTON, N., BLEWITT, M.
721 E., BANNISTER, A. J., KOUZARIDES, T., HUNTLY, B. J., JOHNSTONE, R. W., DREWES, G.,
722 DAWSON, S. J., ARROWSMITH, C. H., GRANDI, P., PRINJHA, R. K. & DAWSON, M. A. 2016.

723 Functional interdependence of BRD4 and DOT1L in MLL leukemia. *Nat Struct Mol Biol,*
724 23**,** 673-81.
725 GODFREY, L., CRUMP, N. T., THORNE, R., LAU, I. J., REPAPI, E., DIMOU, D., SMITH, A. L.,
726 HARMAN, J. R., TELENIUS, J. M., OUDELAAR, A. M., DOWNES, D. J., VYAS, P., HUGHES, J.
727 R. & MILNE, T. A. 2019. DOT1L inhibition reveals a distinct subset of enhancers
728 dependent on H3K79 methylation. *Nat Commun,* 10**,** 2803.
729 HIBI, M., OISHI, S., MATSUSHITA, M., YONESHIRO, T., YAMAGUCHI, T., USUI, C., YASUNAGA, K.,
730 KATSURAGI, Y., KUBOTA, K., TANAKA, S. & SAITO, M. 2016. Brown adipose tissue is
731 involved in diet-induced thermogenesis and whole-body fat utilization in healthy
732 humans. *International Journal of Obesity,* 40**,** 1655-1661.
733 JIMENEZ, M. A., AKERBLAD, P., SIGVARDSSON, M. & ROSEN, E. D. 2007. Critical role for Ebf1 and
734 Ebf2 in the adipogenic transcriptional cascade. *Mol Cell Biol,* 27**,** 743-57.
735 KANG, J. Y., KIM, J. Y., KIM, K. B., PARK, J. W., CHO, H., HAHM, J. Y., CHAE, Y. C., KIM, D., KOOK,
736 H., RHEE, S., HA, N. C. & SEO, S. B. 2018. KDM2B is a histone H3K79 demethylase and
737 induces transcriptional repression via sirtuin-1-mediated chromatin silencing. *FASEB J,*
738 32**,** 5737-5750.
739 KONG, X., BANKS, A., LIU, T., KAZAK, L., RAO, R. R., COHEN, P., WANG, X., YU, S., LO, J. C.,
740 TSENG, Y. H., CYPESS, A. M., XUE, R., KLEINER, S., KANG, S., SPIEGELMAN, B. M. &
741 ROSEN, E. D. 2014. IRF4 is a key thermogenic transcriptional partner of PGC-1alpha. *Cell,*
742 158**,** 69-83.
743 LICHTENBELT, W. D. V., VANHOMMERIG, J. W., SMULDERS, N. M., DROSSAERTS, J. M. A. F. L.,
744 KEMERINK, G. J., BOUVY, N. D., SCHRAUWEN, P. & TEULE, G. J. J. 2009. Cold-Activated
745 Brown Adipose Tissue in Healthy Men (vol 360, pg 1500, 2009). *New England Journal of*
746 *Medicine,* 360**,** 1917-1917.
747 LU, X., SIMON, M. D., CHODAPARAMBIL, J. V., HANSEN, J. C., SHOKAT, K. M. & LUGER, K. 2008.
748 The effect of H3K79 dimethylation and H4K20 trimethylation on nucleosome and
749 chromatin structure. *Nat Struct Mol Biol,* 15**,** 1122-4.
750 MARKENSCOFF-PAPADIMITRIOU, E., ALLEN, W. E., COLQUITT, B. M., GOH, T., MURPHY, K. K.,
751 MONAHAN, K., MOSLEY, C. P., AHITUV, N. & LOMVARDAS, S. 2014. Enhancer interaction
752 networks as a means for singular olfactory receptor expression. *Cell,* 159**,** 543-57.
753 MIER, P., ALANIS-LOBATO, G. & ANDRADE-NAVARRO, M. A. 2017. Protein-protein interactions
754 can be predicted using coiled coil co-evolution patterns. *J Theor Biol,* 412**,** 198-203.
755 MIN, J., FENG, Q., LI, Z., ZHANG, Y. & XU, R. M. 2003. Structure of the catalytic domain of
756 human DOT1L, a non-SET domain nucleosomal histone methyltransferase. *Cell,* 112**,**
757 711-23.
758 NG, H. H., FENG, Q., WANG, H., ERDJUMENT-BROMAGE, H., TEMPST, P., ZHANG, Y. & STRUHL,
759 K. 2002. Lysine methylation within the globular domain of histone H3 by Dot1 is
760 important for telomeric silencing and Sir protein association. *Genes Dev,* 16**,** 1518-27.
761 NGUYEN, A. T. & ZHANG, Y. 2011. The diverse functions of Dot1 and H3K79 methylation. *Genes*
762 *Dev,* 25**,** 1345-58.
763 NGUYEN, H. P., YI, D., LIN, F., VISCARRA, J. A., TABUCHI, C., NGO, K., SHIN, G. W., LEE, A. Y. F.,
764 WANG, Y. H. & SUL, H. S. 2020. Aifm2, a NADH Oxidase, Supports Robust Glycolysis and
765 Is Required for Cold- and Diet-Induced Thermogenesis. *Molecular Cell,* 77**,** 600-+.

766 OKADA, Y., FENG, Q., LIN, Y., JIANG, Q., LI, Y., COFFIELD, V. M., SU, L., XU, G. & ZHANG, Y. 2005.
767 hDOT1L links histone methylation to leukemogenesis. *Cell,* 121**,** 167-78.
768 PUIGSERVER, P., WU, Z., PARK, C. W., GRAVES, R., WRIGHT, M. & SPIEGELMAN, B. M. 1998. A
769 cold-inducible coactivator of nuclear receptors linked to adaptive thermogenesis. *Cell,*
770 92**,** 829-39.
771 RAJAKUMARI, S., WU, J., ISHIBASHI, J., LIM, H. W., GIANG, A. H., WON, K. J., REED, R. R. & SEALE,
772 P. 2013. EBF2 determines and maintains brown adipocyte identity. *Cell Metab,* 17**,** 562-
773 74.
774 SAMBEAT, A., GULYAEVA, O., DEMPERSMIER, J. & SUL, H. S. 2017. Epigenetic Regulation of the
775 Thermogenic Adipose Program. *Trends Endocrinol Metab,* 28**,** 19-31.
776 SAMBEAT, A., GULYAEVA, O., DEMPERSMIER, J., THARP, K. M., STAHL, A., PAUL, S. M. & SUL, H.
777 S. 2016. LSD1 Interacts with Zfp516 to Promote UCP1 Transcription and Brown Fat
778 Program. *Cell Rep,* 15**,** 2536-49.
779 SANCHEZ-GURMACHES, J., HUNG, C. M. & GUERTIN, D. A. 2016. Emerging Complexities in
780 Adipocyte Origins and Identity. *Trends in Cell Biology,* 26**,** 313-326.
781 SCHULZE, J. M., JACKSON, J., NAKANISHI, S., GARDNER, J. M., HENTRICH, T., HAUG, J.,
782 JOHNSTON, M., JASPERSEN, S. L., KOBOR, M. S. & SHILATIFARD, A. 2009. Linking cell
783 cycle to histone modifications: SBF and H2B monoubiquitination machinery and cell-
784 cycle regulation of H3K79 dimethylation. *Mol Cell,* 35**,** 626-41.
785 SEALE, P., BJORK, B., YANG, W., KAJIMURA, S., CHIN, S., KUANG, S., SCIME, A., DEVARAKONDA,
786 S., CONROE, H. M., ERDJUMENT-BROMAGE, H., TEMPST, P., RUDNICKI, M. A., BEIER, D.
787 R. & SPIEGELMAN, B. M. 2008. PRDM16 controls a brown fat/skeletal muscle switch.
788 *Nature,* 454**,** 961-7.
789 SONG, X., YANG, L., WANG, M., GU, Y., YE, B., FAN, Z., XU, R. M. & YANG, N. 2019. A higher-
790 order configuration of the heterodimeric DOT1L-AF10 coiled-coil domains potentiates
791 their leukemogenenic activity. *Proc Natl Acad Sci U S A,* 116**,** 19917-19923.
792 STEGER, D. J., LEFTEROVA, M. I., YING, L., STONESTROM, A. J., SCHUPP, M., ZHUO, D., VAKOC, A.
793 L., KIM, J. E., CHEN, J., LAZAR, M. A., BLOBEL, G. A. & VAKOC, C. R. 2008. DOT1L/KMT4
794 recruitment and H3K79 methylation are ubiquitously coupled with gene transcription in
795 mammalian cells. *Mol Cell Biol,* 28**,** 2825-39.
796 VAN LEEUWEN, F., GAFKEN, P. R. & GOTTSCHLING, D. E. 2002. Dot1p modulates silencing in
797 yeast by methylation of the nucleosome core. *Cell,* 109**,** 745-756.
798 VIRTANEN, K. A., LIDELL, M. E., ORAVA, J., HEGLIND, M., WESTERGREN, R., NIEMI, T.,
799 TAITTONEN, M., LAINE, J., SAVISTO, N. J., ENERBACK, S. & NUUTILA, P. 2009. Functional
800 brown adipose tissue in healthy adults. *N Engl J Med,* 360**,** 1518-25.
801 WANG, W. S. & SEALE, P. 2016. Control of brown and beige fat development. *Nature Reviews*
802 *Molecular Cell Biology,* 17**,** 691-702.
803 WOOD, K., TELLIER, M. & MURPHY, S. 2018. DOT1L and H3K79 Methylation in Transcription and
804 Genomic Stability. *Biomolecules,* 8.
805 YI, D., DEMPERSMIER, J. M., NGUYEN, H. P., VISCARRA, J. A., DINH, J., TABUCHI, C., WANG, Y. &
806 SUL, H. S. 2019. Zc3h10 Acts as a Transcription Factor and Is Phosphorylated to Activate
807 the Thermogenic Program. *Cell Rep,* 29**,** 2621-2633 e4.
808 YI, D., NGUYEN, H. P. & SUL, H. S. 2020. Epigenetic dynamics of the thermogenic gene program
809 of adipocytes. *Biochem J,* 477**,** 1137-1148.